Journal of The Electrochemical Society, **163** (10) H896-H905 (2016)
0013-4651/2016/163(10)/H896/10/$33.00 © The Electrochemical Society

Synthesis and Computational Bandgap Engineering of New 3,4-Alkylenedioxypyrrole (ADOP) Derivatives and Investigation of Their Electrochromic Properties

Gulbin Kurtay,[a] Tugba Soganci,[b] Metin Ak,[b,z] and Mustafa Gullu[a,z]

[a]*Department of Chemistry, Faculty of Science, Ankara University, 06100, Ankara, Turkey*
[b]*Department of Chemistry, Faculty of Art and Science, Pamukkale University, 06100, Ankara, Turkey*

This research highlights the degree of conformity between our electrochemical and theoretical studies conducted on the newly designed electropolymerizable monomers (BuDOP, BenDOP and BenzoDOP) possessing 3,4-alkylenedioxypyrrole (ADOP) backbone (BuDOP). We tried to select logical enhancing of the structures in a stepwise in order to discuss the effects of benzene (BenDOP) and benzodioxane (BenzoDOP) like aromatic subunits to the electrochromic properties of the target monomers. Following to the completion of the synthetic steps, appropriate structural analyses of monomers were performed (FT-IR, GC-MS, ^{1}H-NMR, ^{13}C-NMR). Subsequently, their corresponding polymers were prepared by electrochemical oxidation and characterized. Afterwards, our consecutive efforts have been contributed to theoretical studies in order to obtain information about their structural properties. To this aim, geometry optimizations were carried out using hybrid density functional theory (DFT/B3LYP/LANL2DZ) and HOMO, LUMO energy levels, HOMO-LUMO energy gaps (ΔE), electron affinity (EA) as well as ionization potential (IP) values were calculated. Theoretical data were then used for identifying the structure-electronic properties relationship and we aimed to determine the electrochromic properties of the studied monomers. Our results from the B3LYP/LANL2DZ calculations indicated that P(BenDOP) has the lowest HOMO-LUMO gap and we predicted that theoretical data were in good agreement with the experimental studies.
[DOI: 10.1149/2.0131610jes]

Manuscript submitted May 4, 2016; revised manuscript received June 24, 2016. Published August 3, 2016.

The past forty years have seen increasingly rapid advances in the field of conducting polymers (CPs) and these advanced materials still continue to attract ever-increasing attention.[1–3] In a general point of view, CPs are accepted as pivotal components which open new frontiers in polymeric materials and electronics. Furthermore; optical, mechanical and electrical properties of CPs could be modified under the guidance of rational chemical modification processes in order to bring them desired attributions.[4,5] So they have found a wide range of technological applications in various fields of chemical and biosensors,[6,7] field-effect transistors,[8,9] electrochromic display devices,[10,11] supercapacitors,[12] actuators[13–15] and separation membranes[16–18] as a feasible alternative to metallic or inorganic semiconductor counterparts. These conjugated polymers combine the electrical properties of metals with characteristics of organic polymers that can be tailor-made as per requirements of the applications through modifications of the polymer structure and varying the functional groups in the organic moiety. Thus, the synthesis and characterization of CPs has become a subject of great interest both academic and industrial researchers in diverse domain of science and technology.[19–21]

These conducting organic polymers have been the focus of numerous theoretical and experimental studies since their discovery in 1977.[22,23] One of the goals of the field of CPs is the molecular designing of polymers with tailor-made conduction properties. The main reason is that there is an incomplete understanding of the relationship between the chemical structure of a polymer and its electronic properties.

On the other hand, over the last two decades, the quantum theory of polymers and design of efficient organic CPs have witnessed a growing interest related to their appealing properties.[24,25] Quantum chemistry is expected to play a major role in the development of novel materials with specific and especially predicted electronic and optical properties (structure, bonding, reactivity, etc.).[26,27] In this context, because of their structural simplicity, linear polyenes and polyacetylene have so far been the focus of most of experimental and theoretical studies.[28,29] The detailed understanding of the phenomena occurring on the conjugated chains upon photoexcitation requires the description of the electronic structure of the lowest singlet excited states. This has helped in forgoing a fundamental understanding of the electronic and optical characteristics of the conjugated materials and in guiding the experimental efforts toward novel compounds with enhanced characteristics.[30,31]

3,4-ethylenedioxythiophene (EDOT), 3,4-alkylenedioxypyrrole (ADOP) and their improved derivatives are certainly the most attractive organic conducting polymers due to both their good conductivity and stability properties.[32–35] These compounds are also known as competitors to other existing low band-gap polymers. A large amount of research has been dedicated to the preparation and investigation of properties of EDOT including donor-acceptor-donor type oligomers[36–39] but less has been done about clarifying electronic effects of aromatic ring systems directly substituted on ADOP. On that account, the main purpose of this research is centered around the question of how to explain the effects of benzene and benzodioxane subunits to the electrochromic properties of the conducting polymers of ADOP derivatives. For this reason, as a first step, we have synthesized three inventive 3,4-alkylenedioxypyrrole derivatives; BuDOP, BenDOP and BenzoDOP (Fig. 1). The characterization of the synthesized compounds was carried out by FT-IR, GC-MS, 1H-NMR, 13C-NMR techniques and elemental analysis. Electrochemical polymerizations of the monomers were performed potentiostatically by using acetonitrile (ACN) as solvent and lithium perchlorate ($LiClO_4$) as supporting electrolyte. The polymerizations of the new monomers were performed successfully and effects of the benzene and benzodioxane subunits to the electrical and electrochromic properties of polymers were explained with both experimental and theoretical studies.

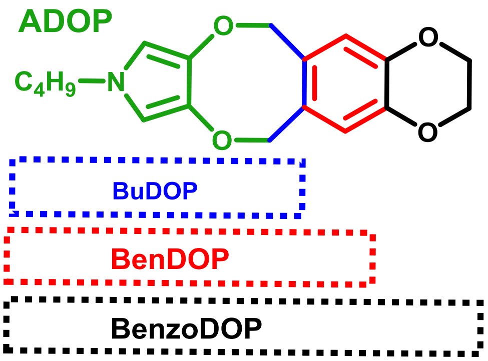

Figure 1. Structure and nomenclature of BuDOP, BenDOP and BenzoDOP monomers.

---

[z] E-mail: metinak@pau.edu.tr; gullu@ankara.edu.tr

Experimental

Materials.—Acetonitrile (Sigma-Aldrich) was pre-dried by shaking with molecular sieves and then distilled over calcium hydride. Similarly; N,N-dimethylformamide (DMF) (*Sigma-Aldrich*) was dried overnight using activated molecular sieves, followed by the decantation of the drying agent and DMF was distilled under vacuum prior to use. Dry ethanol was prepared from magnesium ethoxide. For this purpose, magnesium turnings (10 g) and iodine (1 g) were refluxed in 200 mL of dry ethanol until all of the magnesium reacted. The mixture was diluted (∼1 L) with reagent grade ethanol and refluxed for 3–4 hours then distilled under nitrogen. Anhydrous potassium carbonate (*Fluka*) was pre-dried in an oven at 150°C for 3 to 4 hours. Other dry solvents were stored over a suitable drying agent (frequently type 4A molecular sieves) under oxygen-free nitrogen. Unless otherwise indicated, apiece of the other necessary solvents and reagents used in this study; acetic acid (ReagentPlus, ≥99.5%, *Sigma-Aldrich*), acetone (ACS reagent, ≥99.5%, *Sigma-Aldrich*), benzo-1,4-dioxane (97%, *Aldrich*), benzoyl peroxide (*Sigma-Aldrich*), N-bromosuccinimide (*Sigma-Aldrich*), N-butylamine (*Sigma-Aldrich*), carbon tetrachloride (*Fluka*), 1,4-dibromobutane (99%, *Aldrich*), dichloromethane (DCM) (*Sigma-Aldrich*), diethyl ether (*Sigma-Aldrich*), diethyl oxalate (*Sigma-Aldrich*), ethyl chloroacetate (*Sigma-Aldrich*), hydrogen bromide solution (33 wt% in acetic acid, *Sigma-Aldrich*), hydrogen chloride (ACS reagent, 37%, *Sigma-Aldrich*), lithium perchlorate (*Sigma-Aldrich*), paraformaldehyde (reagent grade, crystalline, *Sigma-Aldrich*), potassium hydroxide (ACS reagent, 85%, *Sigma-Aldrich*), sodium (*Sigma-Aldrich*), sodium sulfate (*Sigma-Aldrich*), triethanolamine (≥ 99.0%, *Sigma*) and o-xylene (*Sigma-Aldrich*) were purchased from their commercial suppliers and used without further purification.

Instrumentation.—In order to accomplish structural characterization of the synthesized compounds, FT-IR spectra were recorded on a Perkin-Elmer Spectrum 100 Series FT-IR spectrometer (*Perkin Elmer Co., Beaconsfield, Bucks, UK*). The samples were prepared by using pressed-pellet (KBr) method or in ATR mode both using the average of 25 scans. Measurements were acquired by scanning the samples from 650 to 4000 cm^{-1} with a resolution of 16 cm^{-1}. GC-MS analyses were conducted using Agilent Technologies 6890N Network GC System and Agilent Technologies 5975B VL MSD Mass Spectrometer (*Agilent Technologies, Santa Clara, CA, USA*) operating at an ionization potential (EI) of 70 eV. ^{1}H-NMR and ^{13}C-NMR spectra (400 MHz) were recorded at room temperature on a Varian Mercury-400 High Performance Digital FT-NMR instrument (Mercury-400BB) (*Varian, Fort Collins, CO, USA*) and $CDCl_3$ was used as solvent. Chemical shifts were reported in parts per million (ppm, δ) relative to tetramethylsilane (TMS, δ: 0) as the internal standard. Proton coupling patterns were described as singlet (s), doublet (d), triplet (t), quartet (q), multiplet (m), and broad (br). Coupling constants J are given in Hz. Melting points (up to 350°C) were determined using an Electrothermal IA9300 digital melting point apparatus and reported uncorrected (*Bibby Scientific Limited*, *OSA, UK*). Elemental analyses were carried out on an Eurovector model EA3000 CHNS elemental analyzer (*EuroVector SpA, Italy*) and found to be within a range of ± 0.4% of theoretical values. Thin layer chromatography (TLC) was used to monitor the progress of the experiments steadily. For this purpose, aluminum sheets (Merck, 20×20, Silica Gel 60 F254) were utilized. Plates were visualized under UV light (at 254 nm) or by staining with iodine. Column chromatography technique was carried out in order to obtain the desired products from common impurities including byproducts and unreacted starting materials. Silica gel (SiO_2) (Merck, Silica Gel 60, 0,063–0.200 mm, 70–230 mesh ASTM) was selected as the column stationary phase. Electrochemical synthesis and cyclic voltammetry experiments performed on a Gamry Reference 600 potentiostat (Gamry Instruments, Warminster, PA, USA) and an Ivium potentiostat/galvanostat (IviumStat, Ivium Tech., The Netherlands). Spectroelectrochemical studies of the resulting polymers were performed with Agilent 8453 UV-vis spectrophotometer (Agilent Technologies, Germany) and indium tin oxide (ITO) coated glass plates of thickness of 0.7 mm with resistance of 8–12 Ω.sq^{-1} (Delta Technologies Limited, USA) were used. All electrochemical experiments were carried out in a one-component cell. The polymer films were deposited electrochemically using ITO-coated plate as working electrode, a Pt counter electrode and pseudo reference electrodes.

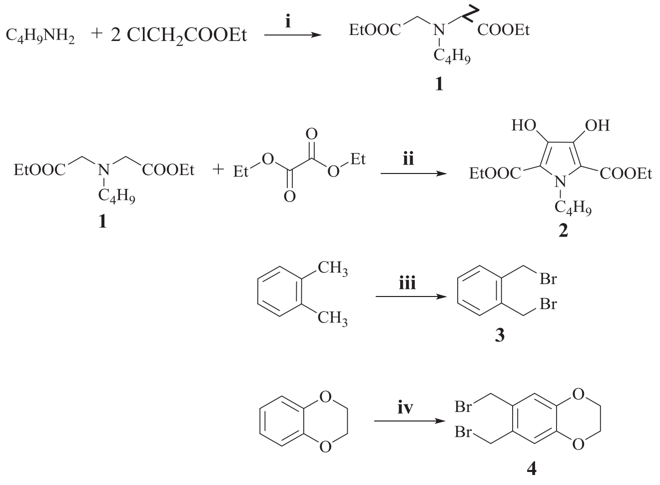

Scheme 1. Synthetic route to the starting materials 2, 3 and 4. Conditions: (i) dry K_2CO_3, ACN, 10 h, 85%; (ii) 1, NaOEt (freshly prepared from Na(s) and EtOH (abs.) under N_2 atmosphere), EtOH, 0°C, diethyl oxalate, 5 h, then treated with glacial acetic acid (pH∼5), 75%; (iii) NBS, CCl_4, reflux, 6 h, 65%; (iv) paraformaldehyde, acetic acid, 0°C, 0.5 h under N_2 atmosphere, then HBr (33 wt% in acetic acid), rt, 24 h, 87%.

Synthetic procedures.— *Synthesis of the starting materials.*—The starting compounds of the target monomers BuDOP, BenDOP and BenzoDOP were obtained by following the synthetic pathway illustrated in Scheme 1.

Diethyl N-butyl iminodiacetate (1): This compound was prepared according to our previously reported method.[19] Firstly, N-butylamine (4.24 g, 5.75 ml, 58 mmol, d: 0.74 g/ml) and dry K_2CO_3 (24.9 g, 180 mmol) in 50 mL of anhydrous acetonitrile were stirred under inert atmosphere at room temperature for 10 minutes. Then, ethyl chloroacetate (13.4 g, 11.7 ml, 110 mmol, d: 1.145 g/ml) was added dropwise to the stirred reaction mixture over a period of 1 hour, following by reflux for 10 hours and ended with TLC monitoring. After cooling the reaction flask to room temperature, the precipitated K_2CO_3 was filtered off and acetonitrile evaporated from the clear filtrate under vacuum at 60°C. The remaining crude product was purified by distillation under reduced pressure to yield 12.90 g (85%) of diethyl N-butyl iminodiacetate as slightly yellow liquid (bp: 230–235°C/ 100–150 mmHg). ^{1}H-NMR (400 MHz, $CDCl_3$) δH/ppm: 0.85 (t, J = 8.1 Hz, 3H, butyl -CH_3), 1.2 (t, J = 7.1 Hz, 3H, ester -CH_3), 1.25 (sextet, J = 7.3 Hz, 2H, butyl -CH_2), 1.4 (p, J = 6.2 Hz, 2H, butyl -CH_2), 2.65 (t, J = 8.0 Hz, CH_2, N-CH_2), 3,5 (t, 2H), 4,1 (q, J = 6,1 Hz, 2H, ester -CH_2). MS (EI) m/z (%) calcd. for $C_{12}H_{23}NO_4$: 245.3; found: 245.2 (M^+, 6), 202 (6.3), 172 (100), 154 (2), 144 (3), 130 (30), 116 (6), 98 (5), 88 (3.5), 59 (7), 42 (15), 29 (5.4). IR (KBr), ν_{max}/cm^{-1}: 2982–2874 (aliphatic C-H), 1747 (ester, C = O), 1467, 1376, 1190 (ester, C-O-C stretching), 1031 (C-N-C stretching), 976, 917.

Diethyl 1-butyl-3,4-dihydroxypyrrole-2,5-dicarboxylate (2): In order to obtain the desired compound, 30 ml of absolute ethanol were carefully added into the reaction flask containing freshly cut sodium metal (1.61 g, 70 mmol) under nitrogen atmosphere. Following to the preparation of the sodium ethoxide solution, the reaction mixture was heated in a hot water bath at 75–80°C and a mixture of diethyl N-butyl iminodiacetate (**1**) (7.36 g, 30 mmol) and diethyl oxalate (4.38 g, 4 ml, 30 mmol, d: 1.076 g/ml) was added dropwise. We observed that the color of the mixture immediately became yellow-brown and after refluxing for 4 hours, formation of a solid yellow chunk was noted.

The reaction mixture was maintained for an additional 1-hour period under the same conditions and then cooled to room temperature. The content of the flask was poured in an ice-water bath and acidified (pH~5) with glacial acetic acid. First of all, the solution became like a milky liquid and then the formation of the crude product has occurred after standing 15 minutes in an ice bath. The solids were separated from the solution by vacuum filtration and purified by recrystallization from ethanol to yield 6.75 g (75%) of diethyl 1-butyl-3,4-dihydroxypyrrole-2,5-dicarboxylate as off-white solid (m.p: 58–60°C). ^{1}H-NMR (400 MHz, $CDCl_3$) δH/ppm: 0.9 (t, J = 7.2 Hz, 3H, butyl -CH_3), 1.3 (sextet, J = 8.0 Hz, 2H, butyl -CH_2), 1.4 (t, J = 6.8 Hz, 3H, ester -CH_3), 1.6 (p, J = 7.6 Hz, 2H, butyl -CH_2), 4.4 (q, J = 7.2 Hz, 2H, ester -CH_2), 4.5 (t, J = 7.8 Hz, 2H, N-CH_2), 7.8 (s, 1H, -OH). MS (EI) m/z (%) calcd. for $C_{14}H_{21}NO_6$: 299.3; found: 299 (M^+, 28), 253 (100), 223 (1,5), 207 (60), 197 (4), 179 (18), 163,9 (94), 150, 0,9 (14), 138 (2), 96 (1,5), 83 (1,8), 69 (4), 57 (5), 44 (78), 28 (22). IR (ATR), ν_{max}/cm^{-1}: 3337, 3248 (O-H stretching), 2984–2864 (z, aliphatic C-H stretching), 1676, 1641 (ester, C = O stretching), 1467–1305 (aliphatic C-H bending), 1262–1126 (ester, C-O-C symmetric and asymmetric stretching), 1023 (C-N-C stretching), 911, 871, 767, 695. Elemental analysis: anal. calcd. for $C_{14}H_{21}NO_6$ (299.3): C 56.18 H 7.07 N 4.68; found: C 55.80 H 6.87 N 4.59.

1,2-Bis(bromomethyl)benzene (3): Synthesis of the brominated compound was achieved in accordance with the literature.[20] For this purpose, o-xylene (5.80 g, 54.0 mmol) and N-bromosuccinimide (NBS) (20.00 g, 112.3 mmol) were dissolved in 25 ml of carbon tetrachloride. A half amount of benzoyl peroxide (0.01 g, 0.04 mmol) was added and heterogeneous reaction mixture started to reflux. After 20 minutes, the other half of benzoyl peroxide (0.01 g, 0.04 mmol) was added and the mixture was refluxed for an additional 6 hours and cooled down to room temperature. In the following step, succinimide solids precipitated during the reaction was separated from the solution under suction and the excess of carbon tetrachloride was removed by vacuum distillation. The crude mixture was chilled in the refrigerator overnight, and the precipitated product was separated by filtration. A white solid was obtained after recrystallization of the crude product from diethyl ether to yield 9.26 g (65%) of 1,2-bis(bromomethyl)benzene (observed m.p: 97°C, lit m.p: 99°C). MS (EI) m/z (%) calcd. for $C_8H_8Br_2$: 264.0; found: 264.0 (M^+, 11), 183.1 (97), 104.2 (100), 78.2 (19).

IR (ATR), ν_{max}/cm^{-1}: 3052–3021 (w, aromatic, C-H stretching), 2965 (w, aliphatic C-H stretching), 1489 (m, aliphatic C-H bending), 768 (s, aromatic C-H bending). Elemental analysis: anal. calcd. for $C_8H_8Br_2$ (264.0): C 36.40 H 3.05 Br 60.54; found: C 35.20 H 2.41.

6,7-Bis(bromomethyl)-2,3-dihydrobenzo[*b*][1,4]dioxine (4): 1, 4-Benzodioxane (2.00 g, 14.7 mmol), paraformaldehyde (0.90 g, 29.4 mmol) and acetic acid (10 ml) were added into a 100 ml round bottomed flask under nitrogen atmosphere and the mixture was stirred in an ice bath for 0.5 hour. Hydrogen bromide solution (33 wt% in acetic acid) was added dropwise into the reaction flask. Afterward, the ice bath was removed and the mixture was allowed to warm to room temperature. The crude product precipitated out from the reaction mixture was purified by flash chromatography on silica gel by elution with dichloromethane. The evaporation of the solvent gave 4.09 g (87%) of white solid product (observed m.p: 138–139°C). ^{1}H-NMR (400 MHz, $CDCl_3$) δH/ppm: 4.20 (s, 4H, -CH_2Br), 4.60 (s, 4H, -CH_2O-), 6.90 (s, 2H, aromatic). MS (EI) m/z (%) calcd. for $C_{10}H_{10}Br_2O_2$: 322.0; found: 322 (M^+, 11), 241 (86), 162 (100), 147 (7), 106 (9), 78 (21). IR (ATR), ν_{max}/cm^{-1}: 3010 (w, aromatic C-H stretching), 2985–2884 (w, aliphatic C-H stretching), 1623, 1509, 1439 (s, aliphatic C-H bending), 1301, 1185, 1065 (s, ether C-O symmetric stretching), 896, 738.

Synthesis of the target monomers.—The target monomers (**BuDOP, BenDOP and BenzoDOP**) were obtained from the reaction of convenient starting materials and corresponding reaction pathway was given at Scheme 2.

Diethyl8-butyl-3,4,5,8-tetrahydro-2H-[1,4]dioxocino[2,3-c]pyrrole-7,9-dicarboxylate (5): In a 100 ml round-bottomed flask, diethyl 1-butyl-3,4-dihydroxypyrrole-2,5-dicarboxylate (**2**) (0.50 g, 1.7 mmol) was added and dissolved in 10 mL anhydrous DMF under nitrogen atmosphere. Following the addition of freshly pre-dried K_2CO_3 (1.10 g, 7.9 mmol), the reaction mixture was stirred vigorously for 0.5 h. Then, 1,4-dibromobutane (0.89 g, 4.1 mmol) was added to the solution and the mixture was heated at 100°C for 6 h. The reaction was followed by TLC and after the termination of the reaction, the excess DMF was distilled off at reduced pressure. The residue was poured into 75 ml ice-water yielding a bright yellow oily solid and the solution was treated with water (1 × 25 ml) and 0.1 N potassium hydroxide solution (2 × 25) to remove unreacted starting material (**2**). The aqueous phase was extracted with DCM (2 × 50 mL) and dried over anhydrous sodium sulfate. The solvent was removed under reduced pressure to give 0.60 g (65%) of diethyl 8-butyl-3,4,5,8-tetrahydro-2H-[1,4]dioxocino[2,3-c]pyrrole-7,9-dicarboxylate (**5**) as bright yellow oily solid. ^{1}H-NMR (400 MHz, $CDCl_3$) δH/ppm: 0.90 (t, 3H, J = 7.6 Hz), 1.31 (sextet, 2H, J = 7.6 Hz), 1.37 (t, 6H, J = 7.2 Hz), 1.65 (p, 2H), 1.93 (s, 4H), 4.06 (t, 4H, J = 5.6 Hz), 4.33 (q, 4H, J = 6.8 Hz), 4.59 (t, 2H, J = 7.6 Hz). MS (EI) m/z (%) calcd. for $C_{18}H_{27}NO_6$: 353.2; found: 353.2 (M+, 36), 308 (15), 280 (100), 253 (16), 238 (8), 224 (5), 206 (8), 197 (7), 168 (6), 150 (9), 55 (11). IR (ATR), ν_{max}/cm^{-1}: 2980–2874 (w, aliphatic C-H stretching), 1711, 1695 (s, ester C = O stretching), 1522, 1435 (s, aliphatic C-H bending), 1308–1255 (s, ester C-O-C asymmetric and symmetric stretching), 1026 (s, ether C-O symmetric stretching), 718.

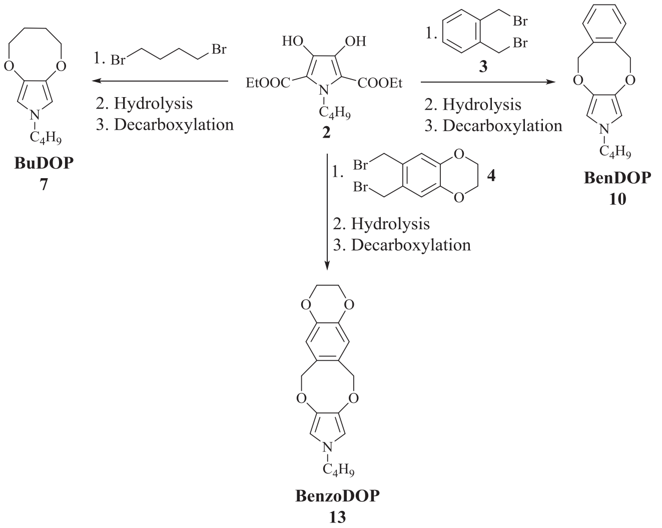

Scheme 2. General procedures for the synthesis of target monomers BuDOP, BenDOP and BenzoDOP.

8-Butyl-3,4,5,8-tetrahydro-2H-[1,4]dioxocino[2,3-c]pyrrole-7, 9-dicarboxylic acid (6): Into a round bottomed flask fitted with a reflux condenser, 8-butyl-3,4,5,8-tetrahydro-2H-[1,4]dioxocino[2,3-c]pyrrole-7,9-dicarboxylate (**5**)(0.50 g, 1.4 mmol) and 15 ml ethanol were added. Following the addition of KOH (85%, 0.34 g, 5.5 mmol) and 1 ml distilled water, the mixture was refluxed in hot water bath for 6 hours. The excess of ethanol was removed by distillation. The unreacted diester derivative (**5**) was separated by extraction with Et_2O and then the residue was mixed with crushed ice. The cooled water phase was acidified with concentrated HCl (pH: 2–3).

The resulting blue-gray colored product was separated by filtration to yield 0.42 g (92%) of 8-butyl-3,4,5,8-tetrahydro-2H-[1,4]dioxocino[2,3-c]pyrrole-7,9-dicarboxylic acid (**6**) (observed m.p: 166–168°C). IR (ATR), ν_{max}/cm-^{1}:3500–2500 (O-H stretching), 2954–2785 (w, aliphatic C-H stretching), 1693, 1651 (s, carboxylic acid C = O stretching), 1435 (m, aliphatic C-H asymmetric bending), 1355 (m, aliphatic C-H symmetric bending), 1263 (s, C-O asymmetric stretching), 1041 (m, C-O symmetric stretching).

8-Butyl-3,4,5,8-tetrahydro-2H-[1,4]dioxocino[2,3-c]pyrrole (7): The corresponding dicarboxylic acid derivative; 8-butyl-3,4,5,8-

tetrahydro-2H-[1,4]dioxocino[2,3-c]pyrrole-7,9-dicarboxylic acid (**6**) (0.50 g, 1.7 mmol) was dissolved in 5 ml triethanolamine. The homogeneous brown solution was stirred under a nitrogen flow in a preheated oil bath at 130°C. The reaction was complete in approximately 30 min as monitored by TLC. The flask content allowed to cool down to room temperature, and mixed with ice-water and then, extracted with DCM, washed with brine and water. Solvent was removed under reduced pressure after drying the organic layer over anhydrous sodium sulfate. The crude product was purified by column chromatography (SiO_2, hexane/ethyl acetate, 2:1, v/v) to give 8-Butyl-3,4,5,8-tetrahydro-2H-[1,4]dioxocino[2,3-c]pyrrole (7) as light yellow oily solid (0.15 g) in 41% yield. ^{1}H-NMR (400 MHz, $CDCl_3$) δH/ppm: 0.90 (t, 3H, J = 7.6 Hz), 1.27 (sextet, 2H, J = 7.6 Hz), 1.64 (p, 2H, J = 7.6 Hz), 1.89 (t, 4H, J = 7.2 Hz), 3.64 (t, 4H, J = 7.2 Hz), 3.94 (t, 2H, J = 6.8 Hz), 6.10 (s, 2H). MS (EI) m/z (%) calcd. for $C_{18}H_{27}NO_6$: 209.2; found: 209.2 (M+, 100), 187 (12), 152 (5), 137 (15.5), 125 (28), 112 (73), 96 (15), 82 (15), 68 (15), 55 (40), 41 (33), 28 (33). IR (ATR), νmax/cm-1: 2934, 2872 (w, aliphatic C-H stretching), 1552, 1409, 1360 (m, aliphatic C-H bending), 1263, 1180 (s, ether C-O symmetric stretching), 732.

Diethyl 2-butyl-5,10-dihydro-2H-benzo[6,7][1,4]dioxocino [2, 3-c]pyrrole-1,3-dicarboxylate (8): Into a 250 ml, two-necked, round-bottomed flask diethyl 1-butyl-3,4-dihydroxypyrrole-2,5-dicarboxylate (2) (1.70 g, 5.68 mmol) was charged and dissolved in 20 ml of dry DMF under nitrogen atmosphere. The oil bath was warmed to 120°C. K_2CO_3 (3.03 g, 21.8 mmol) was added over the solution and stirred for an additional half hour. Afterward, 1,2-bis(bromomethyl)benzene (3) (1.50 g, 5.68 mmol) was added and the mixture was maintained at the same temperature for 6 h. After excess of DMF was removed under reduced pressure, the resulting residue was poured into ice-water and washed with 0.1 N potassium hydroxide solution in order to remove unreacted starting material. The crude product was crystallized from diethyl ether to give desired diester derivative (8) as orange colored solid (1.78 g) in 78% yield (observed m.p: 65–68°C). ^{1}H-NMR (400 MHz, $CDCl_3$) δH/ppm: 0.87 (t, J = 7.6 Hz, 3H, butyl -CH_3), 1.24 (sextet, J = 7.9 Hz, 2H, butyl -CH_2), 1.40 (t J = 6.8 Hz, 6H, ester -CH_3), 1.60 (p, J = 7.6 Hz, 2H, butyl -CH_2), 4.33 (q, J = 7.2 Hz, 4H, ester -CH_2), 4.53 (t, J = 7.8 Hz, 2H, N-CH_2), 5.48 (s, 4H), 7.22 (dd, 2H), 7.34 (dd, 2H). MS (EI) m/z (%) calcd. for $C_{22}H_{27}NO_6$: 401.3; found: 401.3 (M+, 70), 356 (25), 344 (20), 328 (35), 300 (30), 282 (20), 272 (35), 245 (95), 226 (25), 170 (10), 104 (100), 78 (30). IR (ATR), νmax/cm-1: 2987–2870 (w, aliphatic C-H stretching), 1709, 1689 (s, ester C-O stretching), 1438 (m, aliphatic C-H bending), 1312 (m, C-H symmetric bending), 1245 (s, ester C-O-C asymmetric stretching), 1153, 1039 (s, ester C-O-C symmetric stretching), 1025 (s, ether C-O symmetric stretching).

2-Butyl-5,10-dihydro-2H-benzo[6,7][1,4]dioxocino[2,3-c] pyrrole-1,3-dicarboxylic acid (9): Diethyl 2-butyl-5,10-dihydro-2H-benzo[6,7][1,4]dioxocino[2,3-c]pyrrole-1,3-dicarboxylate (8) (0.78 g, 1.94 mmol) was dissolved in 10 ml ethanol, followed by the addition of KOH (85%, 0.33 g, 5.8 mmol), 5 ml EtOH and 1 ml H2O. The mixture was refluxed in hot water bath for 5 hours. Unreacted diester (8) was eliminated by extraction with diethyl ether and then the residue was poured into the crushed ice-water solution. The water phase was acidified with concentrated HCl (pH: 2). The resulting cream colored solids were filtered to yield 0.65 g (97%) of 2-butyl-5,10-dihydro-2H-benzo[6,7][1,4]dioxocino[2,3-c]pyrrole-1,3-dicarboxylic acid (9) (observed m.p: 148–149°C). IR (ATR), ν_{max}/cm-1: 3500-2500 (O-H stretching), 3063 (w, aromatic C-H stretching), 2969–2870 (w, aliphatic C-H stretching), 1687 (s, acidic C-O stretching), 1439 (m, C-H symmetric bending), 1343 (m, C-H asymmetric bending), 1270, 1253, 1239 (s, C-O asymmetric bending), 1041 (m, C-O symmetric stretching).

2-Butyl-5,10-dihydro-2H-benzo[6,7][1,4]dioxocino[2,3-c]pyrrole (10): 2-Butyl-5,10-dihydro-2H-benzo[6,7][1,4]dioxocino[2,3-c]pyrrole-1,3-dicarboxylic acid (**9**) (0.50 g, 1.45 mmol) was dissolved in 5 ml triethanolamine. The solution was stirred under nitrogen atmosphere in a preheated oil bath at 135°C. The reaction was monitored by TLC and completed in 30 min. The mixture allowed to cool down to room temperature and was poured into ice-water. After then, the mixture was extracted with DCM, washed with brine and water, respectively. DCM was removed under reduced pressure and the final product was purified by column chromatography (SiO_2, DCM) to give 2-butyl-5,10-dihydro-2H-benzo[6,7][1,4]dioxocino[2,3-c]pyrrole (**10**) as light gray oily solid (0.16 g) in 43% yield. ^{13}C-NMR (400 MHz, $CDCl_3$) δC/ppm: 13.8, 20.0, 33.4, 50.2, 75.2, 106.1, 128.6, 130.3, 135.8, 136.9.

^{1}H-NMR (400 MHz, $CDCl_3$) δH/ppm: 0.87 (t, J = 7.6 Hz, 3H, butyl -CH_3), 1.23 (sextet, J = 7.9 Hz, 2H, butyl -CH_2), 1.60 (p, J = 7.6 Hz, 2H, butyl -CH_2), 3.57 (t, J = 7.2 Hz, 2H, N-CH_2), 5.29 (s, 4H), 6.10 (s, 2H, pyrrole), 7.25 (m, 4H). MS (EI) m/z (%) calcd. for $C_{16}H_{19}NO_2$: 257.1; found: 257.1(M^+, 100), 186.1 (50), 145.1 (30), 128 (35), 104 (60), 78 (20). IR (ATR), ν_{max}/cm^{-1}: 2958, 2871 (w, aliphatic C-H stretching), 1354 (s, C-H symmetric bending), 1015 (w, ether C-O symmetric stretching).

Diethyl9-butyl-3,6,9,12-tetrahydro-2H-[1,4]dioxino[2″,3″:4′,5′] benzo[1′,2′:6,7][1,4] dioxocino [2,3-c] pyrrole-8,10-dicarboxylate (11): Under nitrogen atmosphere, diethyl 1-butyl-3,4-dihydroxypyrrole-2,5-dicarboxylate (**2**) (1.00 g, 3.3 mmol) was dissolved in 15 ml of pre-dried DMF and heated in oil bath at 120°C for 15 min. K_2CO_3 (2.20 g, 15.8 mmol) was added to the solution and stirred for a half hour. Then, 6,7-bis(bromomethyl)-2,3-dihydrobenzo[b][1,4]dioxine (**4**) (1.28 g, 4.0 mmol) was subsequently added and the mixture was stirred at the same temperature for an additional 8 h. After the completion of the reaction, DMF was evaporated under reduced pressure and the residue was poured into ice-water. The crude product was washed with 0.1 N potassium hydroxide solution to give diester derivative of the target monomer (**11**) as light orange colored solid (1.14 g) in 75% yield (observed m.p: 132–134°C). ^{1}H-NMR (400 MHz, $CDCl_3$) δH/ppm: 0.88 (t, 3H, J = 7.6 Hz), 1.26 (sextet, 2H, J = 7.8 Hz), 1.40 (t, 6H, J = 6.8 Hz), 1.59 (p, 2H, J = 7.6 Hz), 4.24 (s, 4H), 4.34 (q, 2H, J = 7.2 Hz), 4.53 (t, 2H, J = 7.8 Hz), 5.34 (s, 4H), 6.72 (s, 2H, arom.). MS (EI) m/z (%) calcd. for $C_{24}H_{29}NO_8$: 459.2; found: 459.2 (M^+, 8), 414 (7), 386 (33), 358 (20), 340 (20), 330 (25), 247 (11), 162 (100), 147 (11), 106 (18), 78 (26). IR (ATR), νmax/cm-1: 2984-2872 (w, aliphatic C-H stretching), 1703, 1682 (s, ester C = O stretching), 1509, 1439 (s, aliphatic C-H bending), 1300-1243 (s, ester C-O-C asymmetric and symmetric stretching), 1156, 1042 (s, ether C-O symmetric stretching), 884, 776.

9-Butyl-3,6,9,12-tetrahydro-2H-[1,4]dioxino[2″,3″:4′,5′]benzo [1′,2′:6,7][1,4] dioxocino[2,3-c]pyrrole-8,10-dicarboxylic acid (12): Into a 100 ml round bottomed flask fitted with a reflux condenser, diethyl 9-butyl-3,6,9,12-tetrahydro-2H-[1,4]dioxino[2″,3″:4′,5′] benzo[1′,2′:6,7][1,4]dioxocino[2,3-c]pyrrole-8,10-dicarboxylate (**11**) (1.00 g, 2.17 mmol) was dissolved in 15 ml ethyl alcohol. Then, KOH (85%, 0.43 g, 7.6 mmol), 5 ml EtOH and 2 ml H_2O were added into the homogenous solution. The mixture was refluxed for 6 hours. After removal of the excess ethyl alcohol, the solution was cooled to room temperature. The mixture was poured into ice water and then acidified with concentrated HCl and pH was adjusted to 2. The crude product was separated by filtration of the resulting light cream colored solid (0.76 g) in 87% yield (observed m.p: 210°C). IR (ATR), ν_{max}/cm-1: 3400-2500 (O-H stretching), 2988–2901 (w, aliphatic C-H stretching), 1664 (s, acid C = O stretching), 1453 (m, aliphatic C-H asymmetric bending), 1439 (m, C-H symmetric bending), 1303 (s, C-O asymmetric stretching), 1053 (m, C-O symmetric stretching).

9-Butyl-3,6,9,12-tetrahydro-2H-[1,4]dioxino[2″,3″:4′,5′] benzo[1′,2′:6,7][1,4] dioxocino[2,3-c]pyrrole (13): The corresponding dicarboxylic acid derivative; 9-butyl-3,6,9,12-tetrahydro-2H-[1,4]dioxino[2″,3″:4′,5′]benzo[1′,2′:6,7][1,4]dioxocino[2,3-c]pyrrole-8,10-dicarboxylic acid (**12**) (0.50 g, 1.24 mmol) was dissolved in 5 ml triethanolamine. The solution was stirred under a nitrogen flow in a preheated oil bath at 140°C. The reaction was complete in approximately 30 min as monitored by TLC. The flask content allowed to cool down to room temperature, and mixed with ice-water and then, extracted with DCM, washed with brine and water, respectively. DCM was evaporated under reduced pressure after drying the organic layer over anhydrous sodium sulfate. The crude product was purified by column chromatography (SiO_2, DCM) to give the desired monomer (**13**) as yellow oily solid (0.14 g) in 35% yield. ^{13}C-NMR (400 MHz, $CDCl_3$) δC/ppm: 13.8, 20.0, 33.3, 50.2, 64.6, 74.6, 106.2, 119.0, 130.2, 135.9, 143.3. ^{1}H-NMR (400 MHz, $CDCl_3$) δH/ppm: 0.87 (t, J = 7.6 Hz, 3H, butyl -CH_3), 1.23 (sextet, J = 7.9 Hz, 2H, butyl -CH_2), 1.61 (p, J = 7.6 Hz, 2H, butyl -CH_2), 3.58 (t, J = 7.2 Hz, 2H, N-CH_2), 4.22 (s, 4H), 5.15 (s, 4H), 6.10 (s, 2H, pyrrole), 6.74 (s, 2H, benzene). MS (EI) m/z (%) calcd. for $C_{18}H_{21}NO_4$: 315.2; found: 315.2 (M^+, 4), 259.2 (68), 216.1 (35), 203.1 (22), 188.1 (37), 176.1 (44), 162.1 (100), 120.1 (10), 103.1 (10), 96.1 (29), 89.1 (6), 77.1 (7). IR (ATR), ν_{max}/cm-1: 3053 (w, aromatic C-H stretching), 2958–2873 (w, aliphatic C-H stretching), 1300 (s, C-H symmetric bending), 1014 (w, C-O symmetric stretching).

Cyclic voltammetry (CV) studies.—An in-depth analysis of oxidation/reduction behavior of the target monomers and relative prediction of their electroactivity are crucial in order to prepare promising conducting polymers. To this aim, an *Ivium potentiostat/galvanostat* connected to a personal computer (PC) was used in electrochemical measurements. Corresponding cyclic voltammetry studies of BuDOP, BenDOP and BenzoDOP were investigated in a three electrode cell which consisted of a quartz cuvette cell equipped with an indium tin oxide (ITO) coated glass as the working electrode, a platinum wire as the counter electrode and an Ag wire as the pseudo reference electrode. Electrodeposition of the polymers was performed with cyclic voltammetry (CV) technique in 0.1 M $LiClO_4$/ACN (supporting electrolyte/solvent) system. Before the addition of the electropolymerizable monomer, we surveyed a background voltammogram in order to ensure that no impurity was present at the beginning of the electrochemical process.

Spectroelectrochemistry.—Spectroelectrochemical techniques have been widely used to assess the electronic structures and electrochromic properties of the conducting polymers. Therefore, in our experiments, corresponding spectroelectrochemical investigations were conducted via commercially available quartz cuvette (1 cm optical path length) assembled with an optically transparent working electrode, a platinum wire as counter electrode and an Ag wire as pseudo reference electrode. Resultant spectra were collected with a Diode Array UV-vis Spectrophotometer (*Agilent 8453*).

Results and Discussion

Electrochemical properties of polymers.—As mentioned before, electrochemical behavior of the synthesized monomers was investigated through cyclic voltammetry technique. To this purpose, electropolymerization of the monomers was carried out in 0.1 M $LiClO_4$/ACN (supporting electrolyte/solvent) couple at room temperature. Additionally, different potential intervals were applied for each monomer due to their distinct structural properties.

Cyclic voltammetry studies of BuDOP, BenDOP and BenzoDOP.—Electrochemical polymerization experiments were carried out in a three electrode cell containing 0.1 M $LiClO_4$/ACN supporting electrolyte/solvent couple. Cyclic voltammograms of BuDOP, BenDOP and BenzoDOP were then recorded at a potential scan range of −0.3/1.3 V; −0.3/1.0 V and −0.6/1.6 V, respectively (Figure 2).

Hereby, we determined the oxidation and reduction peaks of the corresponding polymers. The cyclic voltammetric data verified the formation of the thin polymeric film on the surface of the working electrode (ITO). On the other hand, in the case of BenzoDOP, although the formation of a tenuous polymer film was observed even with the naked eye, the electrodeposition on the electrode surface could not be achieved steadily. We supposed that this phenomenon might be caused by the formation of short chain-length and bulky structured oligomers of BenzoDOP that could not be deposited on the ITO surface. Hence, P(BenzoDOP) could not be examined in further electrochemical studies conducted within the scope of this work. Howbeit, concomitant comparison of BuDOP and BenDOP revealed that based on the limited intermolecular interactions in BuDOP molecules; even if the polymeric film could be obtained, oligomeric structures tended to desorb from the ITO surface and consequently, we were not able to achieve a well-oriented film coating. However, in conjunction with the addition of the benzene subunit into the monomer backbone (BenDOP); the prevalent π-π stacking interaction between the polymer chains provided a smooth polymerization process. With reference to this information, corresponding electroactive polymers were prepared for all monomers but we detected that BenDOP had remarkable properties when compared with BuDOP and BenzoDOP.

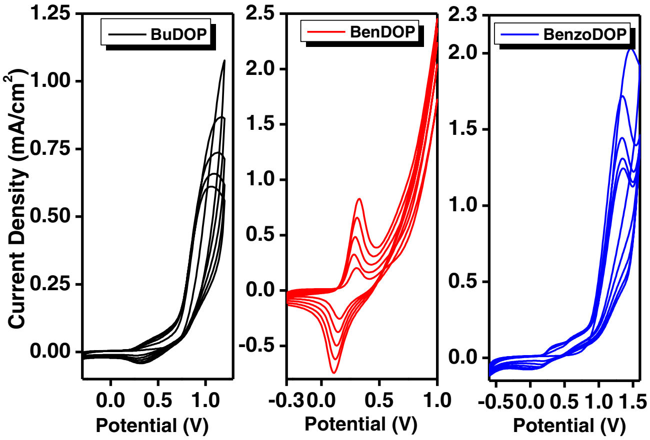

Figure 2. Cyclic voltammogram of BuDOP, BenDOP and BenzoDOP in ACN containing 0.1 M $LiClO_4$ at 250 mV/s scan rate.

Scan rate dependence of the peak currents of BuDOP, BenDOP.—The relationship between the peak current and the scan rate is an appropriate way to the characterization of an electrochemically reversible redox system. In the case of reversible electron transfer, peak currents will increase linearly as a function of the square root of the scan rate. In our study, P(BuDOP) and P(BenDOP) were prepared from their corresponding monomers including $LiClO_4$/ACN supporting electrolyte/solvent system and at constant potential of 1.3 V and 1.0 V, respectively. Afterwards, in order to get information about electroactivities of P(BuDOP) and P(BenDOP) films, the electrochemical behaviors were determined by using cyclic voltammetry at different scan rates in monomer free $LiClO_4$/ACN supporting electrolyte/solvent system as shown in Figure 3.

Hence, the linear dependence of the peak current to the scan rate was accepted as the characteristic response of the electroactive polymer films and proved that P(BuDOP) and P(BenDOP) films were deposited onto the ITO surface. Similarly, linearity of the peak current values indicated that the polymer growth rate was not diffusion-controlled and polymer films could be reversibly oxidized or reduced. Calculated higher r^2 values from the peak current values of P(BenDOP) indicated that this polymer had better adsorption property which shown on during its voltammetric studies.

Besides, HOMO and LUMO energy levels of BuDOP and BenDOP could be calculated by utilizing the onset oxidation potential ($EO_{x(onset)}$) and optical bandgap values on the basis of formula which can be found in literature.[21] Accordingly, in our study, the corresponding HOMO and LUMO energy levels were calculated as 3.24 and 2.38 eV, respectively.

Stability.—Electrochemical stability is accurately related to electrochromic stability because of the degradation of the active redox couple results in the loss of the electrochromic contrast. In order to determine redox stability of the polymer films, P(BenDOP) was electrochemically synthesized between −0.3V and 1.0V potential scan range. Repetitive cyclic voltammetric data of the prepared polymer

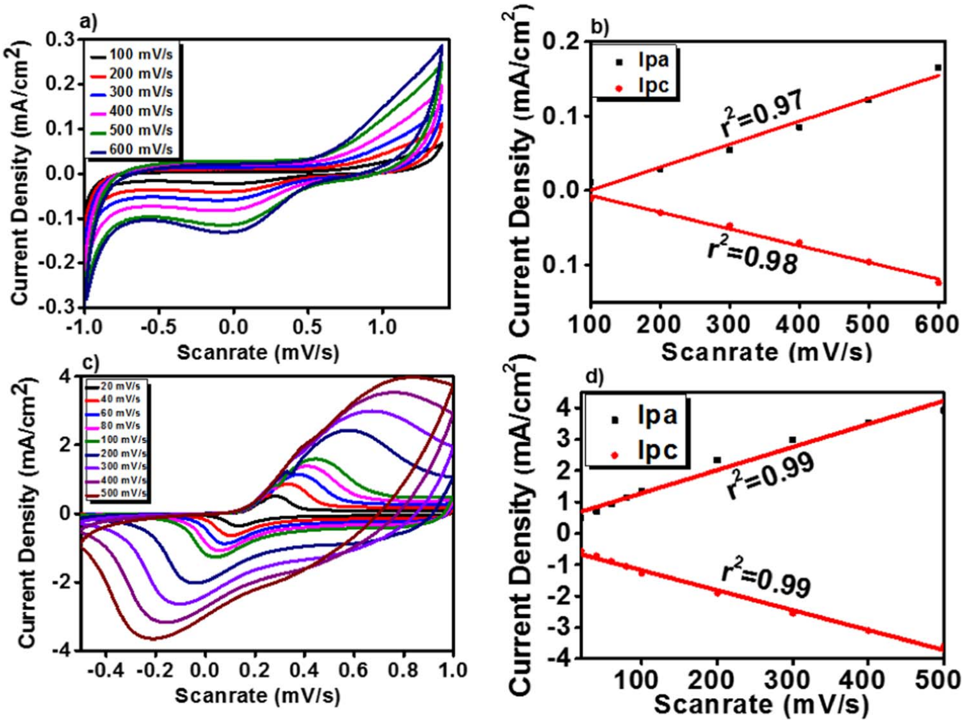

Figure 3. Scan rate dependence of a) P(BuDOP) and c) P(BenDOP) in ACN containing 0.1 M $LiClO_4$. Relation between peak current density and scan rate of the b) P(BuDOP), d) P(BenDOP) film in 0.1 M $LiClO_4$/ACN.

in monomer free $LiClO_4$/ACN supporting electrolyte/solvent system was given at Figure 4.

After 100 cycles it was calculated that there was a decrement about 40% and this result it was determined that P(BenDOP) had a suitable redox and environmental stability.

Electrochromic properties of P(BuDOP), P(BenDOP).— *Spectroelectrochemistry of P(BuDOP) and P(BenDOP).*—Spectroelectrochemistry is a useful method for studying the changes in the absorption spectra when the potential applied. It also provides useful data about the electronic structure of the polymer such as bandgap (E_g) and the intergap states that appear upon doping process. We used ACN as solvent and $LiClO_4$ as supporting electrolyte in order to determine spectroelectrochemical and optical properties of the P(BuDOP) and P(BenzoDOP). P(BuDOP) and P(BenzoDOP) were coated on ITO via constant potential electrolysis and prior to spectroelectrochemical studies, the ITO layer was washed for several times with ACN in order to remove excess of monomer and oligomers. Spectroelectrochemical graphics of P(BuDOP) and P(BenDOP) were shown in Figure 5.

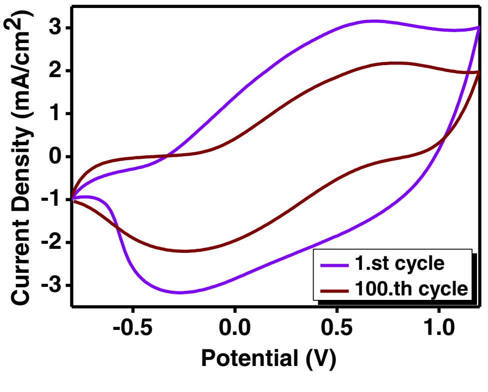

Figure 4. Stability tests of P(BenDOP) via cyclic voltammetry with a scan rate of 250 mV/s 0.1 M $LiClO_4$/ACN.

Accordingly, π-π∗ transition wavelength (λ_{max}) for P(BuDOP) and P(BenDOP) were determined as 309 nm and 395 nm, respectively. The onset energies for the π− π ∗ transition (electronic bandgap) were found to be 3.24 eV for P(BuDOP) and 2.38 eV for P(BenDOP).

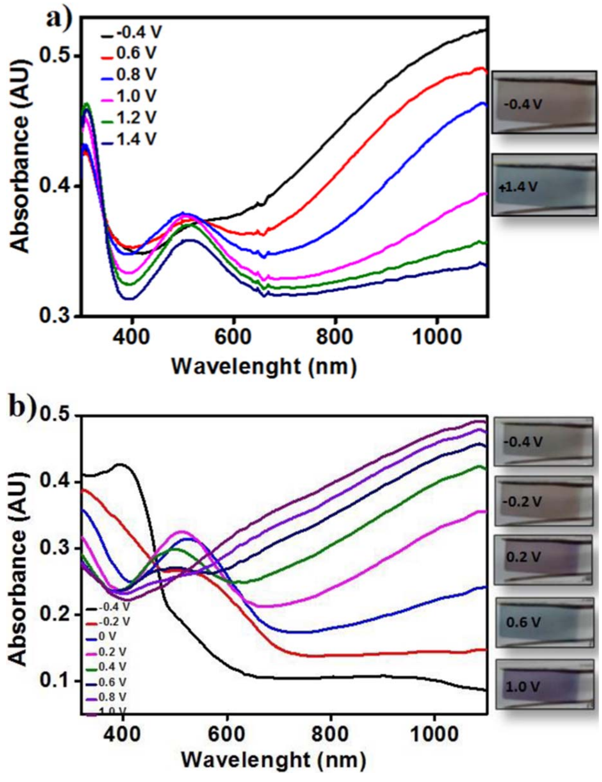

Figure 5. Spectroelectrochemical graphics of a) P(BuDOP), and b) P(BenDOP) 0.1 M $LiClO_4$/ACN.

Table I. The colors and color coordinates of conducting polymers, P(BuDOP) and P(BenDOP) in accordance with the CIE standards.

Polymer	Potential (V)	Luminance (L)	Hue (a)	Saturation (b)
P(BuDOP)	−0.4	94	−9	43
	1.4	94	−9	−7
P(BenDOP)	−0.4	91	−5	31
	−0.2	70	18	4
	0.2	69	8	6
	0.6	65	−24	−4
	1.0	58	−1	−11

Besides, in different potential ranges, the homopolymer of BuDOP was detected in two different colors between light brown to sky blue. On the other hand, we observed five different colors for P(BenDOP) and it showed better spectroelectrochemical properties when compared to P(BuDOP). With this outcome, a valuable multichromic conducting polymer was prepared.

Colorimetry.—The colors of the electrochromic polymers were characterized by performing colorimetry measurements. CIE system was used as a quantitative scale to identify and contrast colors. Three features of color; luminance (L), hue (a), saturation (b) were measured and represented in Table I.

Electrochromic switching.—It is important that polymers can switch rapidly and exhibit striking color changes, revealing superior results in electrochromic applications. A square-wave potential step method coupled with optical spectroscopy was used to study the switching time and contrast of the polymer films. According to this phenomenon, for P(BuDOP); maximum contrast (ΔT%) and switching time (s) were measured from Figure 6a as 12% and 2 s for 1000 nm by adjusting the potential between 0.3 and 1.4 V with a residence time of 5 s. In the case of P(BenDOP); 15% and 1 s for 400 nm; 39% and 1 s for 1000 nm in ACN by adjusting the potential between −0.4 and 1.0 V with a residence time of 5 s (Figure 6b).

Besides this, coloration efficiency (CE) is determined as the change in optical density (OD) per unit charge density (Q_d), which is used for identifying the reduced and the oxidized state of the polymer film and this value applied for obtaining amount of energy which affects to color change. CE can be calculated following the equation in the literature.[22] In our study, Q_d ($Mc.cm^{-2}$) values were calculated by charge-time plots and CE value of P(BuDOP) was found as 94.4 $cm^2.C^{-1}$ at 1000 nm. For P(BenDOP) film, corresponding CE values were found, 55.5 $cm^2.C^{-1}$ at 400 nm and 126.3 $cm^2.C^{-1}$ at 1000 nm, respectively. $T_{colored}$, $T_{bleached}$, OD and CE values were depicted in Table II. The CE values of pyrrole derivatives have ranged from 85 to 250 $cm^2.C^{-1}$ as could be found in literature.[23] When we compared the obtained CE values with the corresponding literature results, we determined that our studied polymers were in acceptable range.

Computational studies.—As mentioned before, the main purpose of this paper is to propound the correlation between the chemical structure and the electronic properties of target monomers as well as their electrochemically synthesized homopolymers. In this regard, computational studies offer a good acquaintance between the molecular properties and the conductivity of the monomers.[24–26] In order to fine-tune optical and electronic properties of conducting polymers, the introduction of substituents at eligible positions of their starting monomers is a frequently used technique.[27–30]

In this study, we have mainly focused on three divergent type of monomers all bearing N-butyl-3,4-butylenedioxypyrrole ring system as the repetition unit. By the inclusion of the butyl substituent on the pyrrole ring's nitrogen atom, we aimed to increase the solubility of the target monomers as well as their corresponding polymers preferably in organic solvents. In light of the preceding theoretical studies, we also expected to obtain a decrease in the positive electrode potentials needed for the electropolymerization.[31] Furthermore, we tried to define the steric hindrance impact between the substituents on the adjacent pyrrole rings liable with the defeat of the effective conjugation and consequently, we focused on the prediction of their effects on the bandgap and molecular energy levels of the target polymers. For these mentioned purposes, the backbone of the first investigated monomer

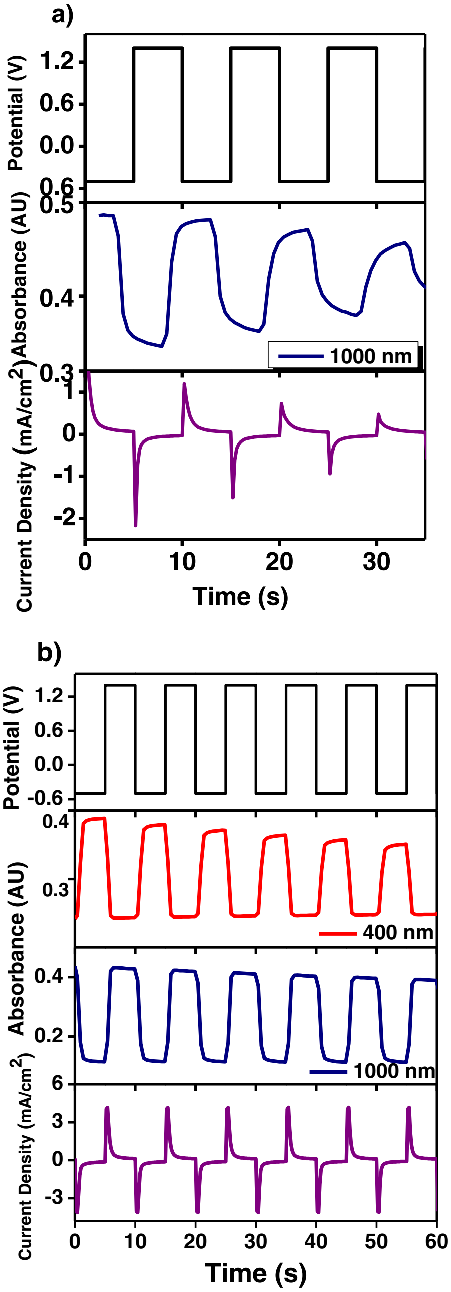

Figure 6. Potential–time, absorbance–time, current density–time graphics for a) P(BuDOP), and b) P(BenDOP) in $LiClO_4$/ACN.

Table II. Optical and electrochemical data collected for coloration efficiency measurements.

Polymer		Q_d ($mC\ cm^{-2}$)	$T_{colored}$; $T_{bleached}$	ΔDO	CE ($cm^2\ C^{-1}$)
BuDOP	1000 nm	1.25	0.432; 0.329	0.118	94.4
BenDOP	400 nm	2.43	0.570; 0.417	0.135	55.5
	1000 nm	2.43	0.765; 0.377	0.307	126.3

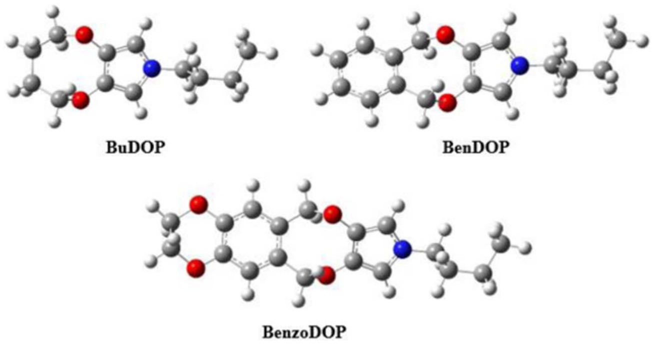

Figure 7. Optimized molecular structures of BuDOP, BenDOP and BenzoDOP obtained by using DFT/B3LYP/LANL2DZ.

(BuDOP) included a pyrrole ring which was cycled between its 3 and 4 positions with flexible butylenedioxy subunit. On the other hand, in the case of BenDOP, we selected to introduce and fuse the benzene substituent on to the monomer backbone under the expectation that the presence of the aromatic ring favors the π-π stacking,[32–35] which could improve the charge mobility and generate a more planar conjugated structure. The last studied monomer, BenzoDOP was designed within the introduction of the benzodioxane subunit to the BuDOP backbone and similar to BenDOP, we wanted to survey the influence of the benzodioxane ring system to the monomer and its corresponding polymer's electronic properties.

The molecular quantum chemical calculations were performed in the gas phase using Density Functional Theory (DFT) implemented in the GAUSSIAN 09 software.[36] The calculations presented here were carried out on single oligomer chain. In other words, the possible influence of the interchain interaction effects were not explicitly taken into account.

***Structural and geometrical parameters.*—**In this part, the equilibrium geometries were calculated by full optimization of the conformations and the electron correlation effects were tested by using the Becke's three-parameter, Lee-Yang-Parr exchange correlation functional (B3LYP) level of calculation with the LANL2DZ basis set[37,38] for BuDOP, BenDOP and BenzoDOP monomers and their corresponding oligomers (n; *number of monomer units*; n:2-5). The choice of this basis set was justified by previous published studies[39,40] where reasonable agreements were found between calculated geometries and experimental data. The geometry optimization studies were performed to evaluate the minimum energy configuration and corresponding optimized structures for target monomers were plotted in Figure 7. All of the calculated structures were visualized with GaussView 5.0 graphics program.[41]

The equilibrium geometry ensured a minimum energy state by checking the second derivatives of energy (NIMAG = 0). Harmonic frequencies obtained were used to calculate the zero-point vibrational energies (ZPVE). The calculations evaluated that there were no significant differences among the obtained bond lengths for all monomers and oligomers in their ground states and the approximate inter-ring distances were about 1.46 A°. The inter-ring torsion angles were also studied and summarized in Table III.

The twisting of the pyrrole backbone was outlined by analyzing the inter-ring torsion angles between two consecutive monomer units and the obtained values were varied from 115 ° to 133 °. As could be easily evaluated from the corresponding data; the optimized geometry of target monomers and oligomers were not totally planar due to the presence of butylenedioxy moieties and the fused aromatic systems on BenDOP and BenzoDOP were oriented in opposite side of their pyrrole ring and its butyl subunit. BuDOP oligomers had lowest inter-ring torsion angles especially at the both ends of the oligomers. Additionally, we observed an appreciable decrease in the inter-ring torsion angles values with the increase of the monomer units. These results were not surprising when considering the greater steric hindrance in BenDOP and BenzoDOP due to the fused benzene and benzodioxane ring systems and their push-pull effect between the pyrrole backbone. It is well known from the previous conformational calculations that the increment of the torsion angles is liable with the increment of the band gaps values.[42] As a consequence, the maximum values of band gaps will be obtained when the torsion angles reach to 90° due to the lack of the π-electron interactions between neighboring monomer units. In other words, potential factors leading to decrease π delocalization across the polymer backbone will end up with an increase in the bandgap. In our study, we attempted to obtain a more planar inter-ring system with the introduction of the benzene and benzodioxane ring systems which could improve stability and conductivity levels by the aid of their resonance energy stabilization through electronic delocalization. Moreover, it is undoubtedly known that the inductive or mesomeric effects of substituents play crucial roles in controlling electronic properties[43] and for this purpose, we proposed to reduce the steric hindrance effects on consecutive monomer units with the aid of the electron-donating oxygen atoms which bridged together in an eight-membered ring system by a butylene group.

***Investigation of Frontier Molecular Orbitals (HOMO and LUMO).*—**The bandgap and molecular energy levels are of pivotal importance for improving electrochromic device performance. It is considered that the electrical properties of conducting polymers are tightly correlated to the energy difference between the Highest Occupied Molecular Orbital (HOMO) and the Lowest Unoccupied Molecular Orbital (LUMO).[44] The relative ordering of the occupied and virtual orbitals ensures a reasonable qualitative indication of the excitation properties as well as the ability of electron or hole transport. The visualization of the molecular orbitals in a qualitative graphical representation, could provide insight into the nature of reactivity, and some of the structural and electronic properties of monomers. For this purpose, in order to analyze electron distribution of HOMO and LUMO energy potentials throughout the monomer units, the contour plots were generated at ground state and depicted in Figure 8.

It could be observed that for all investigated molecules, the shape and spatial electron density of HOMO showed the similar patterns and occupied orbitals mainly localized over the N-butyl-3,4-dioxypyrrole rings and their corresponding π-bonding orbitals. However, the electron density distribution of LUMO was quite different in the case of

Table III. Inter-ring torsion angles of target monomers and their investigated oligomers.

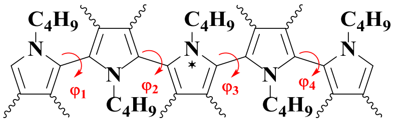

Torsion Angles	n = 2	n = 3		n = 4			n = 5			
	φ_1	φ_1	φ_2	φ_1	φ_2	φ_3	φ_1	φ_2	φ_3	φ_4
BuDOP	−130.12	−120.19	−126.24	−126.58	−116.19	−121.19	−122.62	−114.93	−124.44	−121.31
BenDOP	−129.66	−123.62	−129.25	−129.54	−119.42	−123.56	−129.82	−117.24	−119.26	−123.97
BenzoDOP	−132.88	−122.07	−129.10	−129.69	−118.66	−124.07	−129.46	−117.84	−118.99	−124.74

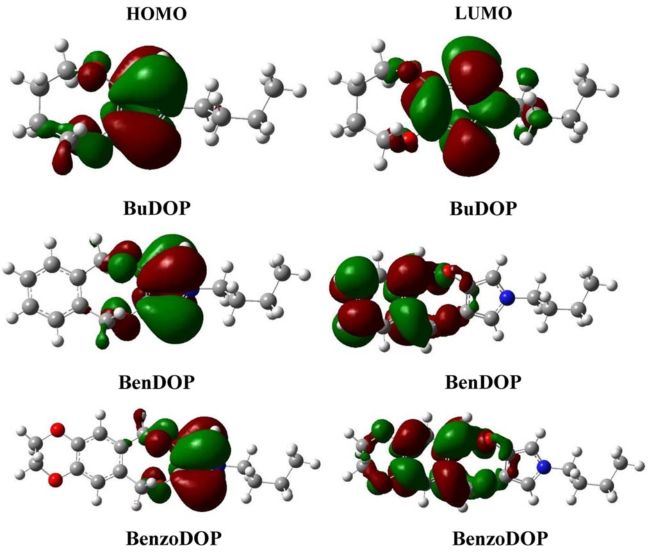

Figure 8. Contour plots of the HOMO and LUMO molecular orbitals of monomers.

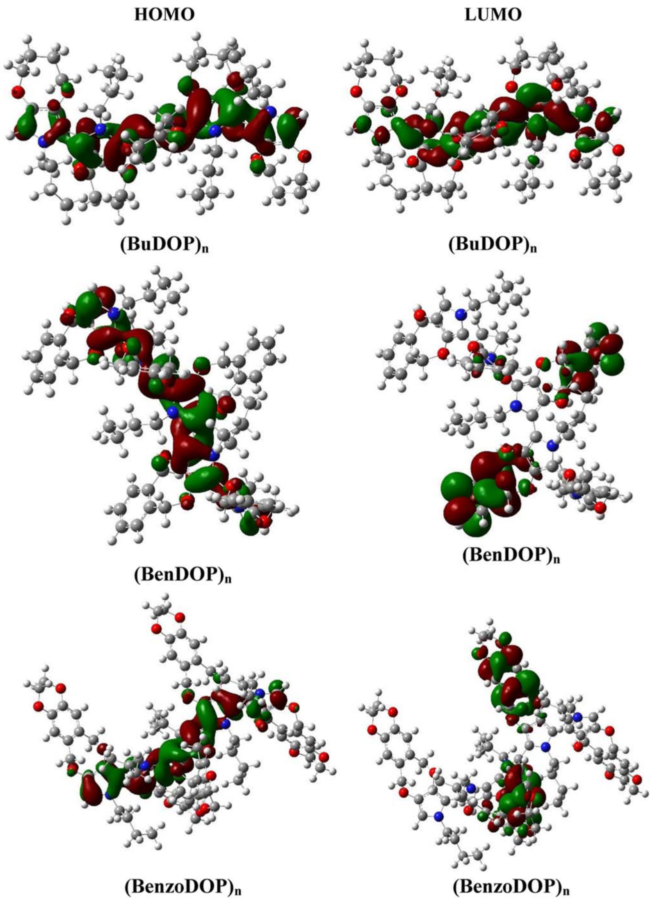

Figure 9. Computed isodensity surface plots of HOMO and LUMO orbitals for BuDOP, BenDOP and BenzoDOP pentamers.

BuDOP due to the absence of a fused aromatic ring system. Additionally, in accordance with our computational studies, we have found that the existence of N-butyl groups on pyrrole ring system does not have a compelling effect on the molecular orbital distribution of BuDOP, BenDOP and BenzoDOP.

Electron density isocontours of HOMO and LUMO of ADOP-based oligomers.—Theoretical isodensity surface plots of the corresponding BuDOP, BenDOP and BenzoDOP oligomers ($n = 5$) were also generated by a similar approach and illustrated in Figure 9. The DFT calculations indicated that the HOMO level had a strong delocalization behavior throughout the oligomer backbone for all investigated molecules. It was found that there was strong π–π interaction between aromatic subunits and pyrrole backbone. However, the LUMO level presented localization with a symmetrical behavior mainly on the benzene and benzodioxane subunits and especially on the central monomer units of the chain for BenDOP and BenzoDOP suggesting efficient charge separation by excitation.

Moreover, HOMO-LUMO band gaps of the polymers (n_∞) were determined by linear extrapolation of the energy values of their oligomers ($n = 2$–5). To this aim, each HOMO and LUMO energy value was plotted against the inverse of the total number of the rings on the oligomer backbone and the intercept at origin (finite number of rings) represents the corresponding bandgap value of the polymer as the degree of polymerization approaches infinity.[40] The calculated HOMO-LUMO band gaps ($\Delta E = E_{LUMO}$-E_{HOMO}) as a function of reciprocal chain length were summarized in Table IV.

Experimental oxidation onset potentials ($E_{onset(ox)}$) of target monomers were predicted by cyclic voltammetry as the position where the oxidation current starts to differ from the baseline. In our case, the obtained values were about 0.63, 0.10 and 0.75 eV for BuDOP, BenDOP and BenzoDOP, respectively. Indeed, the oxidation onset potentials of BuDOP and BenzoDOP were roughly the same and should be used to explain why BuDOP and especially BenzoDOP could not be able to produce a stable polymer film on the surface of working electrode. By the way, the value of BenzoDOP onset potential was predicted more positive than BenDOP, despite the fact that benzodioxane have more π electrons. This leads us to conclude that the additional π electrons in benzodioxane subunits are not involved in extending the π conjugation in the monomer to a dramatic extent.

The bandgap values in BuDOP, BenDOP and BenzoDOP were about 6.26, 4.98 and 5.22, respectively. Upon increasing the number of monomer units the bandgap became smaller and showed convergence. As could be clearly seen from the Table IV, the bandgap value of BenDOP had the narrowest among the other monomers and on the contrary, BuDOP had the highest bandgap value. These results

Table IV. Computed E_{HOMO}, E_{LUMO} and bandgap (ΔE) values of BuDOP, BenDOP and BenzoDOP.

	BuDOP			BenDOP			BenzoDOP		
(eV)	E_{HOMO}	E_{LUMO}	ΔE	E_{HOMO}	E_{LUMO}	ΔE	E_{HOMO}	E_{LUMO}	ΔE
$n = 1$	−5.34	0.92	6.26	−5.54	−0.55	4.98	−5.49	−0.27	5.22
$n = 2$	−4.71	0.40	5.11	−4.93	−0.65	4.28	−4.83	−0.35	4.47
$n = 3$	−4.55	0.33	4.87	−4.73	−0.72	4.01	−4.65	−0.40	4.26
$n = 4$	−4.48	0.33	4.81	−4.68	−0.70	3.97	−4.57	−0.37	4.20
$n = 5$	−4.41	0.33	4.74	−4.66	−0.69	3.97	−4.54	−0.33	4.20
$n = \infty$	−4.17	0.11	4.28	**−4.39**	**−0.76**	**3.64**	−4.26	−0.40	3.87

Table V. Calculated ionization potentials and electron affinity values (eV).

	BuDOP		BenDOP		BenzoDOP	
(eV)	IP	EA	IP	EA	IP	EA
n = 1	5.34	−0.92	5.54	0.55	5.49	0.27
n = 2	4.71	−0.40	4.93	0.65	4.83	0.35
n = 3	4.55	−0.33	4.73	0.72	4.65	0.40
n = 4	4.48	−0.33	4.68	0.70	4.57	0.37
n = 5	4.41	−0.33	4.66	0.69	4.54	0.33
n = ∞	4.17	−0.11	4.39	0.76	4.26	0.40

indicating that benzene subunit on BenDOP had significantly improved hole-creating properties.

Ionization potentials and electron affinities.—Efficient injection and transport of both holes and electrons are important parameters for the rational design of optimized light-emitting diodes. Ionization potentials (IPs) and electron affinities (EAs) are used to estimate the energy barrier for the injection and transport of both holes and electrons into the polymer. It is well known that in simple molecular orbital theory approaches, the HOMO energy (-E_{HOMO}) is related to the IP by Koopmanns' theorem and the LUMO energy (-E_{LUMO}) has been used to estimate the EA values.[45] It should be pointed out that substituents on the polymer chain not only influence the bandgap but also the IP (top of the valence band energy) and the EA (bottom of the conduction band energy). We have developed linear correlation relationships which could be used to semiquantitatively estimate fundamental properties based on the calculated HOMO and LUMO energies and Table V contains the vertical ionization potentials and electron affinities which concern to the geometry of the neutral molecules as functions of reciprocal chain lengths for BuDOP, BenDOP and BenzoDOP (n = 1–5).

The corresponding outcomes showed that with the increase of monomer units, the trend in linearity could be observed for all series (Table V). For instance, the IPs decreased with the increase of the monomer units which indicated that the hole injection properties significantly improved (especially BuDOP) and on the contrary, the EAs increased and reached to a maximum value for BenDOP suggesting the ability to accept electron was promoted (especially BenDOP) and the negative EA values of BuDOP could be explained with the electronically metastable resonance but need further calculations for confirmation.

Conclusions

This research sheds new light on the synthesis, characterization and electropolymerization abilities of the target alkylenedioxypyrrole derivatives; BuDOP, BenDOP, BenzoDOP and we aimed to explore the electrochromic properties of their corresponding polymers. For these purposes, during the electrochemical studies; P(BuDOP) and P(BenDOP) films were successfully obtained on the transparent ITO working electrode surface. However, we explored that after the deposition of the BenDOP monomer, its polymeric film showed excellent electrochemical stability than BuDOP. On the other hand, we observed that BenzoDOP could not be deposited on the ITO surface and we predicted that this might be caused by the steric hindrance effect of the benzodioxane ring system. In theoretical studies, we interpreted the qualitative features by employing the density functional theory (DFT) to attain insight into molecular design; the Becke's three-parameter non-local exchange function with the Lee–Yang–Parr non-local correlation function (B3LYP) is utilized to optimize BuDOP, BenDOP, BenzoDOP monomers and their corresponding oligomers (n = 2–5). All of the studied compounds have no imaginary frequencies at the present level, which implies that all the optimized structures are the steady points on the potential energy surface and LANL2DZ was used as basis set. The linearity between the calculated properties and the reciprocal chain length is excellent for the homologous series of oligomers. Theoretical band gaps including directly calculated ionization potential (IP) and electron affinity (EA) values were in good agreement with the available experimental studies. Additionally, our results from the B3LYP/LANL2DZ calculations indicated that P(BenDOP) has the lowest bandgap and it could be considered as a promising candidate for electronic, opto-electronic and photovoltaic applications.

Acknowledgments

One of the researchers (Metin Ak) gratefully thanks to the Scientific and Technological Research Council of Turkey (TÜBİTAK; project number: 111T074). Mustafa Güllü and Gülbin Kurtay also would like to express their gratitude to TÜBİTAK (TBAG/110T071) and AU-BAP (14H0430002) for their financial supports.

References

1. T. K. Das and S. Prusty, *Polym. Plast. Technol. Eng.*, **51**, 1487 (2012).
2. I. Yağmur, M. Ak, and A. Bayrakceken, *Smart Mater. Struct.*, **22**, 115022 (2013).
3. R. J. Mortimer, *Electrochim. Acta*, **44**, 2971 (1999).
4. L. Groenendaal, F. Jonas, D. Freitag, H. Pielartzik, and J. R. Reynolds, *Adv. Mater.*, **12**, 481 (2000).
5. I. Giurgiu et al., *Synth. Met.*, **119**, 405 (2001).
6. M. Gerard, A. Chaubey, and B. D. Malhotra, *Biosens. Bioelectron.*, **17**, 345 (2002).
7. U. Lange, N. V. Roznyatovskaya, and V. M. Mirsky, *Anal. Chim. Acta*, **614**, 1 (2008).
8. H. Koezuka and A. Tsumura, *Synth. Met.*, **28**, 753 (1989).
9. J. W. Schultze and H. Karabulut, *Electrochim. Acta*, **50**, 1739 (2005).
10. K. Hyodo, *Electrochim. Acta*, **39**, 265 (1994).
11. R. J. Mortimer, A. L. Dyer, and J. R. Reynolds, *Displays*, **27**, 2 (2006).
12. G. A. Snook, P. Kao, and A. S. Best, *J. Power Sources*, **196**, 1 (2011).
13. A. Della Santa, D. De Rossi, and A. Mazzoldi, *Synth. Met.*, **90**, 93 (1997).
14. a Della Santa, D. De Rossi, and a. Mazzoldi, *Smart Mater. Struct.*, **6**, 23 (1999).
15. M. Fuchiwaki, K. Tanaka, and K. Kaneto, *Sensors Actuators, A Phys.*, **150**, 272 (2009).
16. J. Bobacka, *Electroanalysis*, **18**, 7 (2006).
17. H. Zhang, S. Salinas, and V. B. Sundaresan, *Smart Mater. Struct.*, **20**, 094020 (2011).
18. F. Faridbod, M. R. Ganjali, R. Dinarvand, and P. Norouzi, *Sensors*, **8**, 2331 (2008).
19. G. Kurtay, M. Ak, M. Güllü, L. Toppare, and M. S. Ak, *Synth. Met.*, **194**, 19 (2014).
20. H. J. Dauben and L. L. McCoy, *J. Am. Chem. Soc.*, **81**, 4863 (1959).
21. E. Zhou et al., *Macromolecules*, **41**, 8302 (2008).
22. C. L. Gaupp, D. M. Welsh, R. D. Rauh, and J. R. Reynolds, *Chem. Mater.*, **14**, 3964 (2002).
23. P. Camurlu, *RSC Adv.*, **4**, 55832 (2014).
24. J. Casado, V. Hernandez, F. J. Ram??rez, and J. T. Lopez Navarrete, *J. Mol. Struct. THEOCHEM*, **463**, 211 (1999).
25. J. Fabian and H. Hartmann, *Dye. Pigment.*, **79**, 126 (2008).
26. A. Raya and M. A. Mora, *Polymer (Guildf).*, **45**, 6391 (2004).
27. M. M. Oliva et al., *J. Org. Chem.*, **71**, 7509 (2006).
28. R. M. Osuna, X. Zhang, A. J. Matzger, V. Hern??ndez, and J. T. L. Navarrete, *J. Phys. Chem. A*, **110**, 5058 (2006).
29. X. Q. Ran et al., *J. Phys. Chem. A*, **112**, 10904 (2008).
30. S. M. Bouzzine et al., *J. Phys. Chem. A*, **116**, 9730 (2012).
31. X. Huang et al., *J. Phys. Chem. C*, **119**, 27247 (2015).
32. J. W. G. Bloom and S. E. Wheeler, *Angew. Chemie - Int. Ed.*, **50**, 7847 (2011).
33. S. L. Cockroft et al., *Org. Biomol. Chem.*, **5**, 1062 (2007).
34. C. a Hunter and J. K. M. Sanders, *J. Am. Chem. Soc.*, **112**, 5525 (1990).
35. J. Hwang et al., *J. Am. Chem. Soc.*, **136**, 14060 (2014).
36. D. J. Frisch, M. J. Trucks, G.W. Schlegel, H. B. Scuseria, G. E. Robb, M. A. Cheeseman, J. R. Scalmani, G. Barone, B. Petersson V.;Mennucci, G. A. Nakatsuji, H. Caricato, M. Li, X. Hratchian, H. P. Izmaylov, A. F. Bloino, J. Zheng, and G. Sonnenber, *Gaussian, Inc. Wallingford CT*, 2 (2009).
37. S. Chiodo, N. Russo, and E. Sicilia, *J. Chem. Phys.*, **125** (2006).
38. J. Roncali, *Chem. Rev.*, **97**, 173 (1997).
39. H. Kayi, *J. Mol. Model.*, **20**, 2269 (2014).
40. S. Yang, P. Olishevski, and M. Kertesz, *Synth. Met.*, **141**, 171 (2004).
41. T. K and J. M. Roy Dennington, *Semichem Inc., Shawnee Mission KS*, (2009).
42. M. Wykes, B. Milián-Medina, and J. Gierschner, *Front. Chem.*, **1** (2013).
43. R. Daengngern and N. Kungwan, *J. Lumin.*, **167**, 132 (2015).
44. S. S. Zade and M. Bendikov, *Org. Lett.*, **8**, 5243 (2006).
45. C.-G. Zhan, J. A. Nichols, and D. A. Dixon, *J. Phys. Chem. A*, **107**, 4184 (2003).